NASA TECHNICAL MEMORANDUM

NASA TM X-52259

NASA TM X-52259

THE DISTRIBUTION OF NEUTRAL ATOMS AND CHARGE-EXCHANGE IONS DOWNSTREAM OF AN ION THRUSTOR

by John F. Staggs, William P. Gula, and William R. Kerslake
Lewis Research Center
Cleveland, Ohio

TECHNICAL PAPER proposed for presentation at Fifth Aerospace Sciences Meeting sponsored by the American Institute of Aeronautics and Astronautics
New York, New York, January 23-27, 1967

NATIONAL AERONAUTICS AND SPACE ADMINISTRATION · WASHINGTON, D.C. · 1966

THE DISTRIBUTION OF NEUTRAL ATOMS AND CHARGE-EXCHANGE IONS DOWNSTREAM OF AN ION THRUSTOR

by John F. Staggs, William P. Gula, and William R. Kerslake

Lewis Research Center
Cleveland, Ohio

TECHNICAL PAPER proposed for presentation at
Fifth Aerospace Sciences Meeting sponsored by the
American Institute of Aeronautics and Astronautics
New York, New York, January 23-27, 1967

NATIONAL AERONAUTICS AND SPACE ADMINISTRATION

THE DISTRIBUTION OF NEUTRAL ATOMS AND CHARGE-EXCHANGE IONS DOWNSTREAM OF AN ION THRUSTOR

by John F. Staggs, William P. Gula, and William R. Kerslake

Lewis Research Center
National Aeronautics and Space Administration
Cleveland, Ohio

ABSTRACT

In a practical design of an electric-propulsion space vehicle, it is likely that some components, such as a solar-cell array, will be exposed in some degree to neutral atoms and charge-exchange ions leaving the thrustors. The purpose of this paper is to describe the energy and angular distributions of such particles emerging from a 15 cm diameter mercury electron-bombardment thrustor. An analytical approach was used to determine the particle effluxes. The results indicate that the erosion and/or coatings due to charge-exchange ions or neutral particle effluxes would be tolerable for several years if components were located outside the primary ion beam and at distances of 75 cm or greater from the thrustor. The value of 75 cm was chosen to simplify the analytical solution. At distances much closer than 75 cm a more detailed study would be required because the thrustor can no longer be accurately represented as a point source. Approximate scaling relations are given that should allow rough determination of particle effluxes for various combinations of nominal operating parameters other than those used in this study.

INTRODUCTION

Electric propulsion is becoming more attractive for a variety of spaceflight missions as a result of improvements in thrustor performance and component technology. For example, an interesting design study has been made recently to investigate the feasibility of electric propulsion systems for unmanned probes (ref. 1). One of the possible problems found in the course of such design studies concerns the relative placement of thrustors with respect to the solar-cell arrays or other spacecraft components (ref. 2). If the spacecraft is designed for maximum compactness and minimum weight, it is likely that the solar-cell array will be exposed to some amount of neutral atoms and/or ions leaving the thrustor. The major directed part of the ion beam is easily avoided. However, the "edge" of the beam is not well defined due to the presence of charge-exchange ions in the thrustor exhaust. In recent long duration tests, neutralizers were mounted in regions outside the major directed ion beam and they experienced appreciable ion erosion (ref. 3). The extent of the damage was found to decrease as the radial distance from the beam axis increased. Thus, the problem arises of defining regions in which possible neutral particle coatings and/or ion erosion will be at an acceptable level. Of course, acceptable levels must be determined from considering the mission duration, the spectrum of particles leaving the thrustors, and the properties of the spacecraft structure hit by these particles.

The purpose of this paper is to describe the theoretical energy and angular distribution of neutral atoms and charge-exchange ions leaving a 15 centimeter diameter, mercury electron bombardment thrustor. Because the magnitudes of these quantities are small, accurate experimental measurements are very difficult. However, the processes giving rise to such effluxes are fairly well understood so that an analytical approach may be used. Although the results obtained are not precise, they are adequate for initial spacecraft design calculations. In addition, they serve to indicate which aspects of the problem may deserve more detailed study.

Model and General Approach

The thrustor used as the basis of this study is described in reference 3 and shown in figure 1. At normal operating conditions the beam current from this thrustor is 250 mA, extracted with a screen voltage of 3 kV and an accelerator voltage of -2 kV. With 511 holes in the electrodes, the average current per hole is about 0.49 mA. The extracted current distribution across the thrustor is such that at the center the maximum current per hole is about 1.0 mA, or about twice the average value. The current extracted from the outer perimeter holes is about 0.25 mA per hole. The thrustor is normally operated at a propellant utilization efficiency of 80 percent. Anode wall temperature is about 500° K, resulting in a neutral atom temperature in the discharge chamber of about the same value.

For the analysis, the possible charge-excharge ions were grouped as follows:

(1) those leaving the thrustor with dispersion angles between 0° and 20° (considered to be within the primary ion beam)

(2) those leaving the thrustor with dispersion angles between 20° and 90°

(3) those returning to the thrustor and impinging on the accelerator electrode

(4) those produced downstream of the neutralization plane and not returning to the thrustor

The ions in groups (2) and (4) were of prime interest for this study, since these ions may impinge on surfaces downstream of the thrustor. Figure 2 shows typical trajectories of the four groups of charge-exchange ions and the approximate region of origin. The zero volt equipotential line, which falls between the screen and accelerator, was regarded as the downstream boundary of the formation region for the group (2) ions. This was because any ion formed at a negative potential would return to the thrustor.

The electrode configuration shown in figure 2 represents one hole of the thrustor extraction system. The potential at the trajectory starting point prescribes the potential energy of the ion formed at that point. The angle between the centerline and a tangent to the trajectory at the point where the ion

enters the neutralized exhaust plasma was used to determine the angular distribution of the charge-exchange ions. The formation of the group 4 charge-exchange ions in the region downstream of the neutralization plane was treated as a separate problem and will be discussed later.

The charge-exchange analysis was made using an IBM 7094 digital computer program (ref. 4) and an electrolytic tank analog (ref. 5) in a combined manner described in detail in reference 6. Briefly, the technique involves determining the Poisson potential distribution of the desired model using the digital computer program, then establishing this distribution in the electrolytic tank. (With this method the potential distribution of an axially symmetric model is readily established in a simple two-dimensional (flat bottom) tray of the electrolytic tank analog.) Once the proper distribution has been established, the exhaust beam is arbitrarily divided into a number of mesh squares. Charge exchange ion trajectories are then started with zero initial velocity from the centers of these mesh squares and traced on an X-Y plotter. The local charge-exchange ion production rate is then calculated as follows. The charge-exchange ion production rate in an element of volume is

$$\dot{N} = Q\dot{n}n_0 \Delta L\, a \qquad (1)$$

where Q is the cross section for charge-exchange (the value 6×10^{-15} cm^2 was used for mercury). (All symbols are defined in appendix A.) The elements of volume in this case are toroidal with square cross section ($a = 2\pi\bar{r}\,\Delta L$, where $\bar{r}$ is the average radius of the toroid).

The primary ion arrival rate $\dot{n}$, was calculated by a technique similar to the one used in determining charge contribution of flowing ions to elements of volume in reference 5. In brief, the primary ion flow is divided into stream tubes (the ion trajectories are the stream tube boundaries). The current flowing in each stream tube is known from the digital computer solution. The ion arrival rate at a particular volume element is thus determined by summing the contributions from all the stream tubes intercepted by the volume element.

The neutral atom density, n_0, was assumed to be uniform in the interelectrode region and extending downstream as far as the neutralization plane. A value was obtained from the relation

$$n_0 = \frac{\mu_0 ta}{V} = \frac{\mu_0 ta}{A\,\Delta L} = \frac{\mu_0 a}{Av} \qquad (2)$$

where μ_0 is the rate at which neutrals leave the screen aperture, A is the area of a screen hole, and v is the r.m.s. velocity of a neutral atom at 500° K. The assumption of a uniform neutral density for the entire extraction system implies that the propellant utilization efficiency per hole varies since the current density per hole is not uniform. The total charge-exchange ion production rate in the interelectrode region was determined by summing all the local contributions calculated by equation (1). Results were obtained for a few typical cases and are presented in the RESULTS AND DISCUSSION section. In order to generalize the results to cover other cases, the effect of changing various thrustor parameters on the charge-exchange ion production was examined. The resulting scaling relations are given in appendix B.

RESULTS AND DISCUSSION

Charge-Exchange Ions

The charge-exchange ion analysis was performed for three different values of current extracted from a single hole in the electrode. The current values were approximately chosen to represent extraction from a typical outer hole, midsection hole, and central hole of a thrustor operating at a beam current of 250 mA. The specific values used for individual hole currents were 0.230 mA, 0.435 mA, and 1.034 mA, respectively, with corresponding propellant utilization efficiencies of approximately 65, 80, and 90 percent. Figure 3 shows the results obtained for group 2 charge exchange ions for the high current, central hole case. Part (a) of the figure shows some typical charge-exchange ion trajectories. In part (b) the charge-exchange ion formation region is shown divided into subregions which produce ions in an indicated range of dispersion angles. No subregion is shown producing ions with dispersion angles above 44°. This lack of detail is a result of the mesh size used. Actually, there will be a distribution of ions between 45° and 90° dispersion angles that originate in the downstream half of the two subregions near the axis on the right. These ions, however, would have very low energies since the zero volt equipotential is very close to the region at that point. Also not indicated, due to the coarseness of the mesh used, is a narrow region near the centerline of the hole where the ions formed will have dispersion angles less than 20° (group (1) type). In part (c) of figure 3 the charge-exchange ion formation region is divided into subregions that produce ions in a particular energy range.

Results for the midsection and outer hole were somewhat similar in appearance to figure 3. It was interesting to learn, however, that the maximum dispersion angle of the primary ion beam was largest for the outer hole. This is a result of "crossover" trajectories (ref. 5) rather than simple beam spreading. It was previously thought that the primary ion beam boundary existed at approximately a 15° dispersion angle; however, this study and the long duration tests on thrustors indicate that a low primary ion flux continues out to about a 20° dispersion angle.

The results of the analysis are presented graphically in figures 4 and 5. Figure 4 shows the average number of group (2) ions within a particular range of dispersion angles. In all three cases most of the ions leave the thrustor at relatively low dispersion angles. Figure 5 shows group (2) ion energies versus dispersion angle. The solid curves represent the maximum energies determined and the dashed curves are an extrapolation of the solid curves to the 90° dispersion angle. The shaded regions cover the areas in which all the values of this analysis occurred. Charge-exchange ions will be produced with energies filling the remainder of the area under the curves, but they will be relatively small in number.

The groups (1) and (3) charge-exchange ions were determined in number only (i.e., specific dispersion angles, or, impact points on the accelerator for the group (3) ions were not recorded). The total number of these charge-exchange ions was calculated using equation (1). The results obtained for the first three groups of charge-exchange ions are

summarized in table I. From the table it can be seen that the total charge-exchange ion current from groups (1), (2), and (3) ions was about 0.4 percent of the total beam current. Of this total charge-exchange ion current, 84 percent impinged on the accelerator (group (3)), 10 percent escaped with the primary beam (group (1)), and 6 percent escaped with a dispersion angle between 20° and 90° (group (2)). Figure 6 shows the total charge-exchange ion flux for group (2) ions as a function of dispersion angle. In preparing this graph it was assumed that the thrustor could be regarded as a point source. A distance equal to about five thrustor diameters (75 cm) seems sufficient for this purpose.

To calculate the group (4) charge-exchange ions (those produced in the region downstream of the neutralization plane), the following assumptions were made: (1) neutrals are emitted uniformly over the thrustor diameter and follow a cosine law of divergence, (2) the ion flux leaving the accelerator grid is paraxial, remains paraxial, and is of uniform density. The simplifying assumption of no beam spreading results in negligible error of total number of charge-exchange ions produced because: (a) neutral density does not change appreciably in the region between 0° and 20° beam dispersion, and (b) the same number of primary ions are considered in either case.

A radial neutral density distribution was calculated for several distances downstream of the thrustor using equation (6) of reference 8. The result of these calculations are shown in figure 7. The densities have been normalized to the value of neutral density at the neutralization plane. The neutral flux gradients that would occur near the thrustor because of the grid structure were assumed to blend into a smooth profile approximately 3 centimeters downstream.

Once the neutral density distribution is determined, the calculation of the charge-exchange ion formation rate at various locations can be made using equation (1). The calculation was made using the thrustor operating conditions of 80 percent propellant utilization efficiency, 0.250 ampere beam current, and 3000 volts net accelerating voltage. A value of 6×10^{-15} cm^2 was used for Q. The result is plotted in figure 8 as the number of ions per cm^2 per second passing through the wall of a cylinder equivalent in shape to the assumed primary ion beam (see sketch of cylinder on fig. 8). Each charge exchange ion was assumed to travel radially and normal to the axis at the beam. This assumption seems valid for the reasons given below. The charge-exchange ion has only random thermal ($\sim 500^{\circ}$ K) energy when it is formed. Any electric fields existing in the ion beam will dictate the direction of travel of the charge-exchange ions. Reference 9 indicates that the predominate (although small) electric field in the ion beam will be radial. The energy gained by a charge-exchange ion leaving a well neutralized beam is probably less than about 50 volts. Figure 8 indicates that the maximum number of group 4 ions will be found near the thrustor. The decreasing number found further away from the thrustor is, of course, due to the diminishing neutral efflux.

Effects on Spacecraft Components

In order to give an idea of the possible affects of the neutral atom effluxes and group (2) and (4) charge-exchange ions on spacecraft components two different shaped surfaces located downstream of the thrustor were considered as intercepting these effluxes. The first surface was a cylinder, concentric with the primary beam, and with a diameter of 150 centimeters or 10 times the thrustor diameter (see fig. 9(a)). The primary ion beam was assumed to spread with a dispersion angle of 20°. The length of the cylinder was chosen so as to just intercept the primary ion beam. The second surface was a plane, normal to the thrustor axis, 75 cm downstream and with a hole to allow the primary ion beam to pass through (see fig. 9(b)).

A distance of 75 centimeters seemed adequate for this purpose so that the thrustor could be regarded as a point source. Figure 10 shows the distribution of the total ion flux of group (2) and group (4) charge-exchange ions arriving at the cylindrical surface as a function of dispersion angle. The highest flux occurs at low dispersion angles going down to a minimum flux between 45° and 50° dispersion, and then rising again at high dispersion angles due to the increasing contribution of group (4) ion fluxes.

The flux arriving at the planar surface normal to the thrustor axis is entirely due to the group (2) charge-exchange ions. Figure 10 also shows the distribution of this flux as a function of dispersion angle. The highest flux again occurs at low dispersion angles, dropping to zero at the higher dispersion angles.

The charge-exchange ion flux arriving at the surfaces used in the previous calculation can vary from zero to about 10^{11} particles per cm^2 per second. Their energy range is from 0 to about 2.5 kV. In comparison, cosmic radiation flux in deep space is about 2.5 particles per cm^2 per second (refs. 10, 11, and 12). This flux consists mainly of protons with energies from 10 to 10^{12} MeV. On the other hand the proton flux in the Van Allen belts ranges up to 10^9 protons per cm^2 per second with an energy range from 0.1 keV to 700 MeV (refs. 10, 11, and 12). Damage to solar cells by the natural radiation flux is caused primarily by the penetration of the high energy particles into the cell itself which can cause a degradation in performance. The flux from the thrustor does not possess sufficient energy to penetrate a shield such as a 0.1 millimeter thickness of quartz commonly used to protect the cell from natural radiation. Rather it seems likely that any damage done by the thrustor efflux would be a result of sputtering erosion. If a sputtering yield of one particle per incident ion for mercury on quartz (refs. 13 and 14) and a flux of 10^{11} ions per cm^2 per second is assumed, the resulting wear rate is 3.8×10^{-13} centimeters per second. The wear rate of silver, assuming a sputtering yield of seven atoms per incident ion (refs. 13 and 14) and a flux of 10^{11} ions per cm^2 per second is 5.87×10^{-13} cm/sec. Most materials have wear rates between these two values. At these wear rates it would take 1.8×10^6 hours to wear away one-quarter of a 0.1 millimeter thick quartz shield. Of course, this wear rate would increase for components located closer to the thrustor.

The neutral flux was calculated by assuming a

uniform flux across the surface of the accelerator grid, a cosine distribution for the dispersion, and a total flow of 3.9×10^{17} neutrals per second which corresponds to the operating conditions used in this study. Figure 11 shows the distribution of neutral particles intercepted by the cylindrical and planar surfaces shown in figure 9. The energy of the neutrals is below the sputtering threshold energy, therefore the most probable effect of these neutrals would be film deposition. Thus, it becomes important to compare the arrival rate of neutrals with their evaporation rate at the assumed conditions. The evaporation rate relation is

$$n_0 = \frac{P}{(2\pi mkT)^{1/2}} \qquad (3)$$

Assuming a temperature of 330° K for the component (ref. 15), this corresponds to an equilibrium vapor pressure for mercury of 2×10^{-2} torr. At these conditions, the evaporation rate is 2.73×10^{18} particles/cm^2 per second. Comparing this value with the values on figure 11, it can be seen that the possibility of forming a coating on these surfaces, other than a chemisorbed monolayer, is indeed remote. For cesium propellant the evaporation rate would be approximately three orders of magnitude less. For the arrival fluxes calculated, this lower evaporation rate is still enough to preclude coating.

CONCLUSIONS

The results of this study indicate that the effects of charge-exchange ions and neutral particle effluxes from a 15 centimeter diameter mercury, electron-bombardment ion thrustor on spacecraft components will be minimum outside the primary ion beam and at distances of at least 75 centimeters from the thrustor. Under the assumed conditions, silver, for example, would wear at a rate of 3.8×10^{-13} centimeters per second and quartz would wear at a rate of 5.87×10^{-13} centimeters per second. For most components this wear rate should be tolerable for missions of less than 100,000 hours. At distances much closer than 75 centimeters a more detailed study would be required because at these closer distances the thrustor cannot be accurately represented as a point source.

Coating of components with neutral mercury atoms should not be a problem at distances of at least 75 centimeters since the particle effluxes are about seven orders of magnitude lower than the evaporation rate at an assumed component temperature of 330° K.

The approximate scaling relations given in ap appendix B should allow rough determination of particle effluxes for various combinations of operating parameters other than those used in this study.

APPENDIX A

SYMBOLS

A	area of screen hole
a	cross sectional area of volume element
k	Boltzmann constant
ΔL	incremental length
m	mass
$\dot{N}$	charge-exchange ion formation rate
$\dot{n}$	ion arrival rate
n_0	neutral atom density
$\dot{n}_0$	neutral atom evaporation rate
P	pressure
Q	charge-exchange cross-section
$\bar{r}$	average radius of torroid
T	temperature
t	time
V	volume
v	velocity
η_u	propellant utilization efficiency
μ_0	arrival rate of neutrals
φ	electric potential

APPENDIX B

SCALING RELATIONS

Scaling relations were developed by considering "equivalent cases." Two cases were considered equivalent if their potential distributions as determined from digital computer analysis were similar in shape and if the location of the zero volt equipotential line was about the same in each case. The concept of equivalent cases is useful in that all trajectories, both those of primary ions and charge-exchange ions, follow identical paths. To begin, several cases of interest are first run on the digital computer to obtain potential distributions. Charge-exchange currents are then determined. Now, suppose a solution is desired for a case that has a different combination of operating parameters than any of the ones previously run. This new case is first run on the digital to obtain a potential distribution. The previous cases are examined for one which is "equivalent" to the new case. Then by using the scaling relations given below it is possible to determine approximate values of the charge-exchange currents. The scaling parameters developed in general apply only to electron bombardment thrustors.

Propellant Utilization Efficiency

An expression relating the primary ion flow rate $\dot{n}$, the neutral atom arrival rate μ_0, and the propellant utilization efficiency η_u is as follows:

$$\mu_0 = (1 - \eta_u)\frac{\dot{n}}{\eta_u} \qquad (B1)$$

Now, from equations (1), (2), and (B1)

$$\dot{N} \propto \mu_0 \propto \frac{1 - \eta_u}{\eta_u}$$

where $\dot{N}$ is the number of charge-exchange ions generated in any one of the three groups upstream of the neutralization plane. The scaling relation is then,

$$\frac{\dot{N}_1}{\dot{N}_2} = \frac{\eta_{u_2}(1 - \eta_{u_1})}{\eta_{u_1}(1 - \eta_{u_2})} \tag{B2}$$

Particle Temperature

From equations (1) and (2)

$$\dot{N} \propto \frac{1}{v}$$

and since $v \propto (T)^{1/2}$, where T is the temperature of the particle,

$$\dot{N} \propto \frac{1}{(T)^{1/2}}$$

so that

$$\frac{\dot{N}_1}{\dot{N}_2} = \left(\frac{T_2}{T_1}\right)^{1/2} \tag{B3}$$

Accelerating Voltage

For a given thrustor size, the Child's law relation shows that $n \propto \varphi^{3/2}$, where φ is accelerating voltage. Equations (2) and (B1) show that $n_0 \propto \dot{n}$. Since from equation (1), $N \propto n_0\dot{n}$, then

$$\dot{N} \propto \varphi^3$$

or

$$\frac{\dot{N}_1}{\dot{N}_2} = \left(\frac{\varphi_1}{\varphi_2}\right)^3 \tag{B4}$$

provided that the same fraction of space-charge-limited current flow is maintained in both cases.

Propellant

A change of propellant corresponds to a change of the charge-to-mass ratio of the ions, assuming singly charged particles. In "equivalent" cases currents will differ since, according to Child's law, $\dot{n} \propto m^{-1/2}$ where m is the mass of the ions. From equation (1)

$$\dot{N} \propto Q\dot{n}n_0$$

however, n_0 is independent of m, so that

$$\dot{N} \propto Q\dot{n} \propto Qm^{-1/2}$$

or

$$\frac{N_1}{N_2} = \frac{Q_1}{Q_2}\left(\frac{m_2}{m_1}\right)^{1/2} \tag{B5}$$

provided that the same fraction of space-charge-limited current flow is maintained.

REFERENCES

1. Anon., "Solar powered electric propulsion spacecraft study," Hughes Aircraft Company, Space Systems Div. Report No. SSD-50094R, NASA CR-71185 (December 1965).

2. Ratcheson, W. I., "Fabrication feasibility study of a 20 watt per pound solar cell array," Boeing Company Report No. D2-23942-5, NASA CR-70582 (November 1965).

3. Reader, P. D., "Durability tests of mercury electron-bombardment ion thrustors," AIAA Paper No. 66-231 (March 1966).

4. Bogart, C. D. and Richley, E. A., "Space-charge-flow computer program," NASA TN D-3394 (April 1966).

5. Staggs, J. F., "An electrolytic tank analog for two-dimensional analysis of electrostatic-thrustor optics," NASA TN D-2083,(May 1965).

6. Staggs, J. F., Richley, E. A., and Gula, William P., "Ion extractor system design," proposed AIAA Journal Note, accepted Oct. 1966.

7. Cook, H. and Richley, E. A., "Measurements of efflux patterns and flow rates from cylindrical tubes in free-molecule and slip flows," NASA TN D-2480 (September 1964).

8. Reynolds, T. W. and Richley, E. A., "Thermionic emission from cesium-coated electrostatic ion-thrustor electrodes," NASA TN D-1879 (September 1963).

9. Sellen, J. M., Jr., Kemp, R. F., and Hieber, R. H., "Observations of neutralized ion thrust beams in the 25-meter NASA testing chamber," Section III G of TRW Space Technology Lab. Report No. 8003-6037-SU-000, NASA CR 53634 (April 1964).

10. Vosteen, L. F., "Environmental problems of space flight structures. I. Ionizing radiation in space and its influence on spacecraft design," NASA TN D-1474 (October 1962).

11. Davis, D. D., Jr., "Space environment and its effects on materials," Proceedings of the NASA-University Conference on the Science and Technology of Space Exploration, NASA SP-11, vol. 2 (December 1962), pp. 439-449.

12. Foelsche, T., "Current estimates of radiation doses in space," NASA TN D-1267 (July 1962).

13. Wehner, G. K., "Sputtering yields for normally incident Hg^+-ion bombardment at low ion energy," Phys. Rev., 108, 35-45 (1957).

14. Wehner, G. K., "Low-energy sputtering yields in Hg," Phys. Rev., 112, 1120-1124 (1958).

15. Thekaekara, M. P., "Survey of the literature on the solar constant and the spectral distribution of solar radiant flux," NASA SP-74 (1965).

TABLE I. - GROUP (1), (2), AND (3) CHARGE-EXCHANGE ION PRODUCTION.

Exhaust beam region	Current per hole, mA/hole	Number of holes allocated	Primary beam current, mA	Propellant utilization efficiency	Charge-exchange ion current, mA			
					Group (1)	Group (2)	Group (3)	Total
Central	1.034	85	87.9	0.90	0.016	0.018	0.330	0.364
Midsection	0.435	256	111.4	0.80	0.048	0.026	0.330	0.404
Outer	0.230	170	39.1	0.65	0.026	0.008	0.120	0.154
Total	-	511	238.4	0.80	0.090	0.052	0.780	0.922

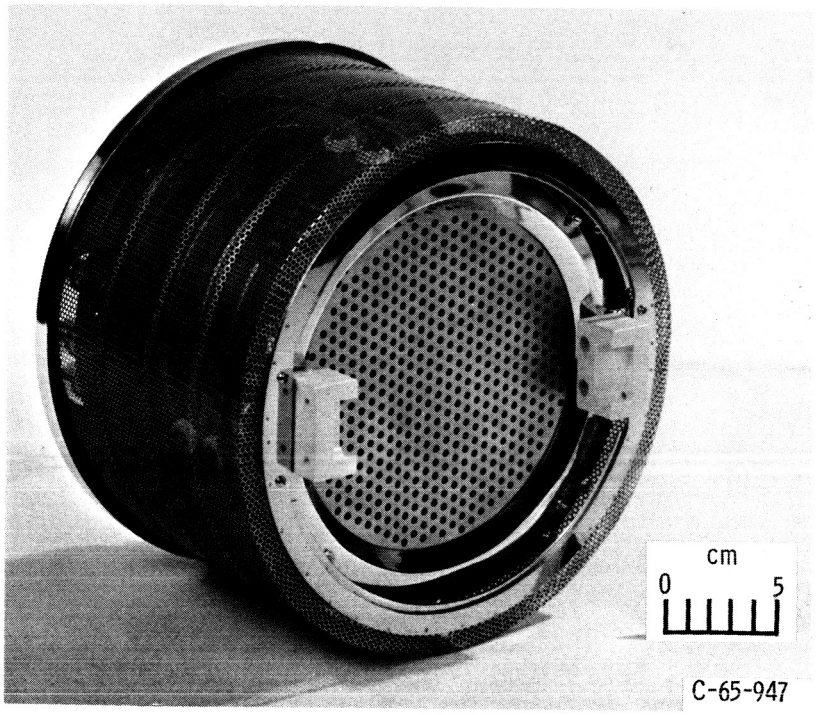

Fig. 1. - Electron bombardment ion thrustor.

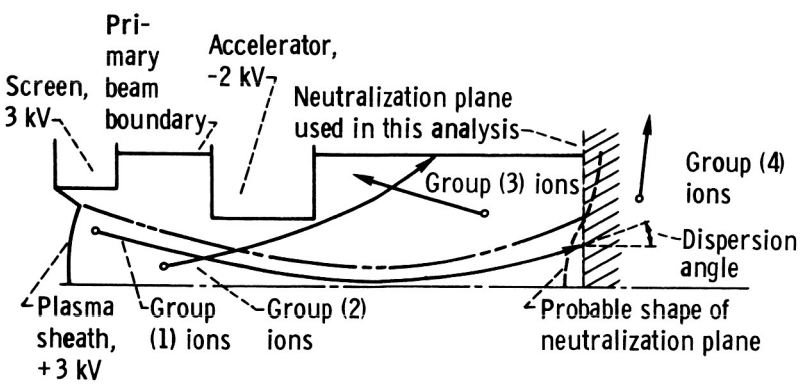

Figure 2. - Electrode configuration showing the four groups of charge-exchange ions.

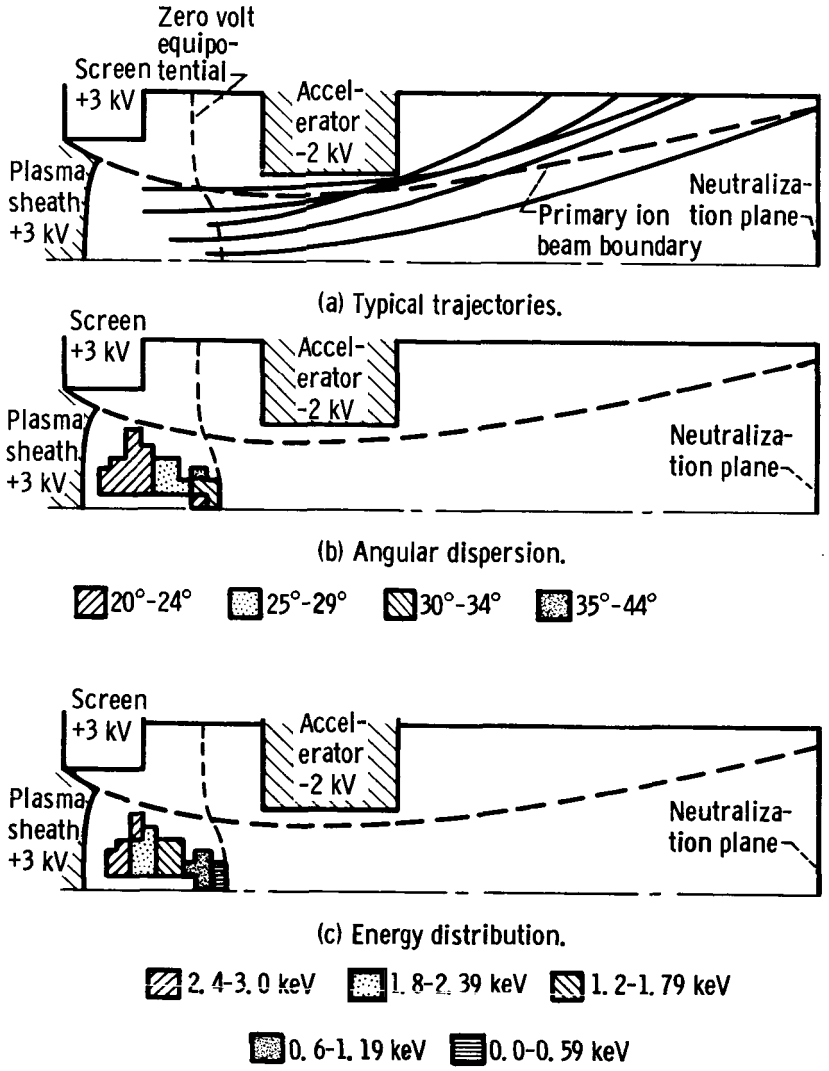

Figure 3. - Charge-exchange ion formation for group (2) ions with a central hole. Primary ion current of 1.034 mA. Propellant utilization, 90 percent.

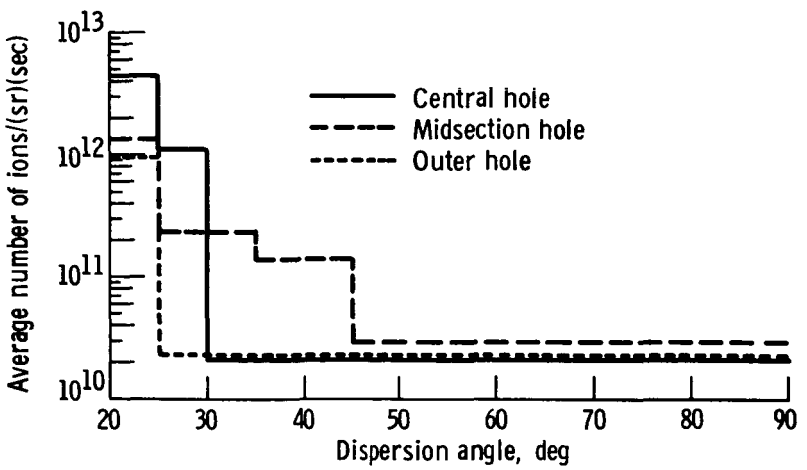

Figure 4. - Number of group (2) ions against dispersion angle.

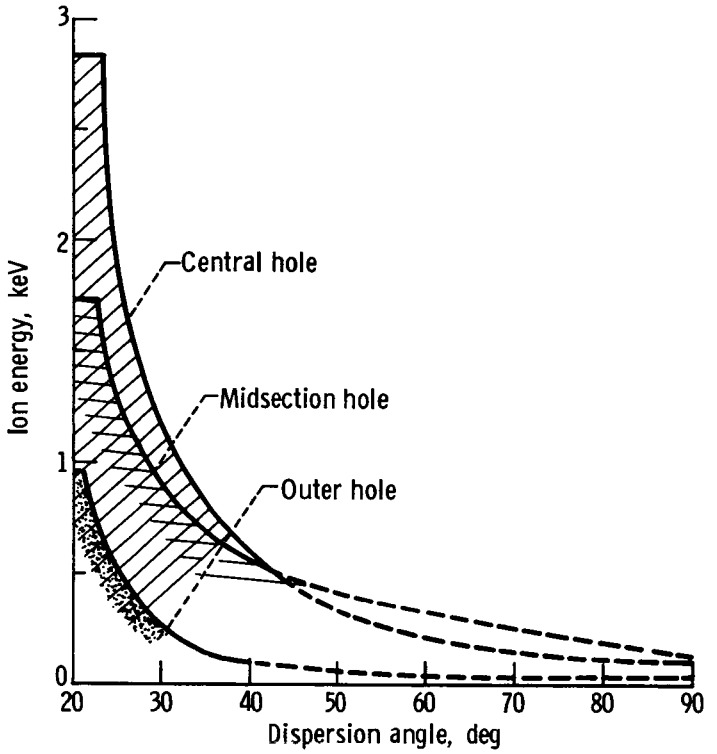

Figure 5. - Group (2) charge-exchange ion energy against dispersion angle.

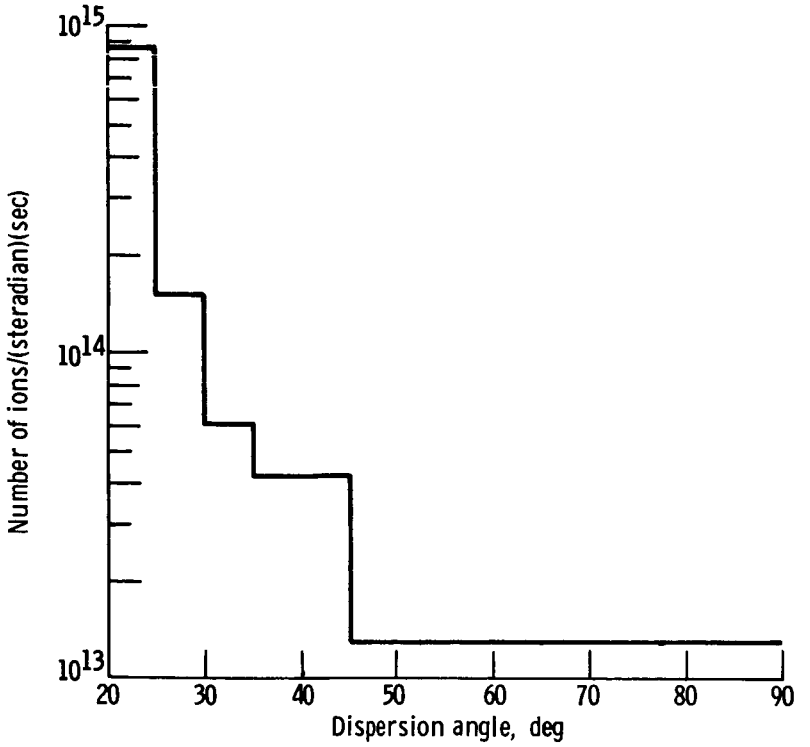

Figure 6. - Total group (2) charge-exchange ions escaping thruster.

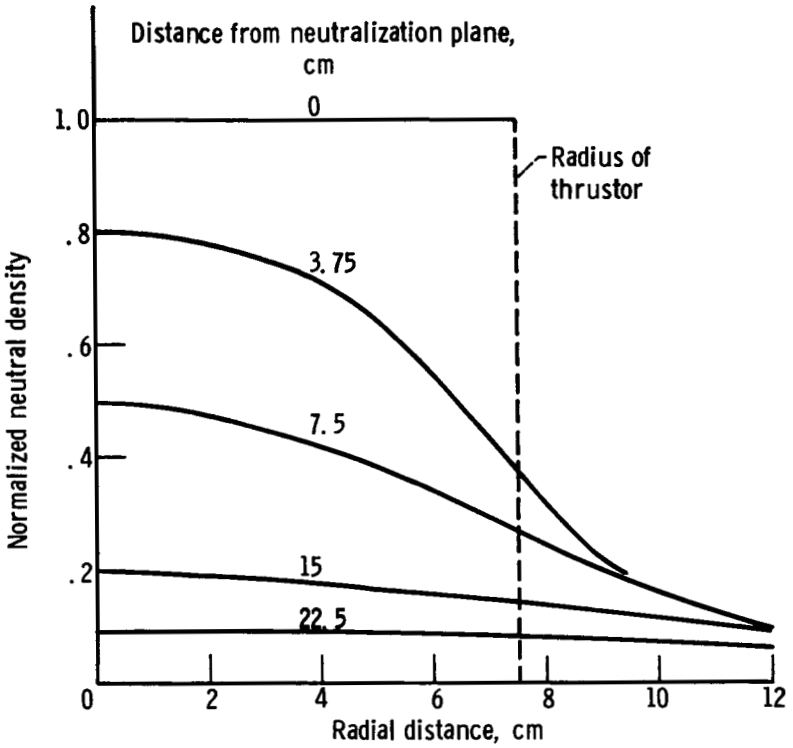

Figure 7. - Calculated values of neutral density for various distances downstream of neutralization plane.

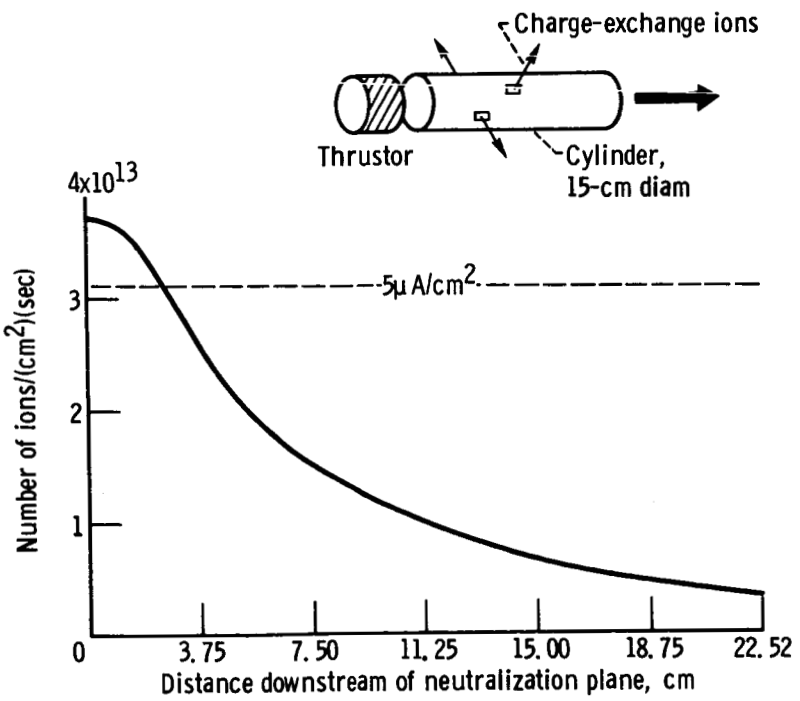

Figure 8. - Calculated values of group (4) charge-exchange ions passing through the surface of a 15-centimeter diameter cylinder, the assumed primary ion beam boundary.

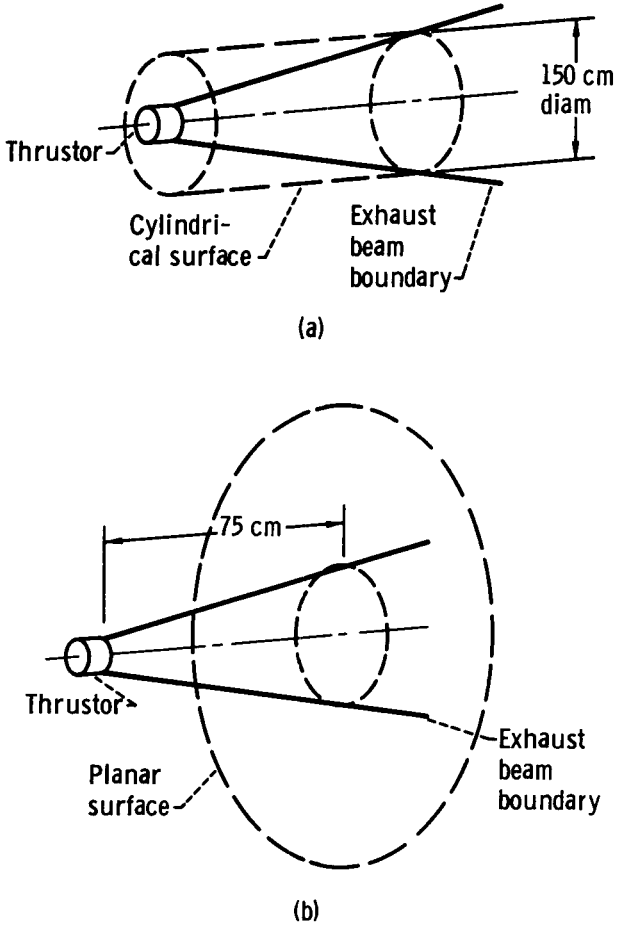

Figure 9. - Two surfaces considered as intercepting thrustor fluxes.

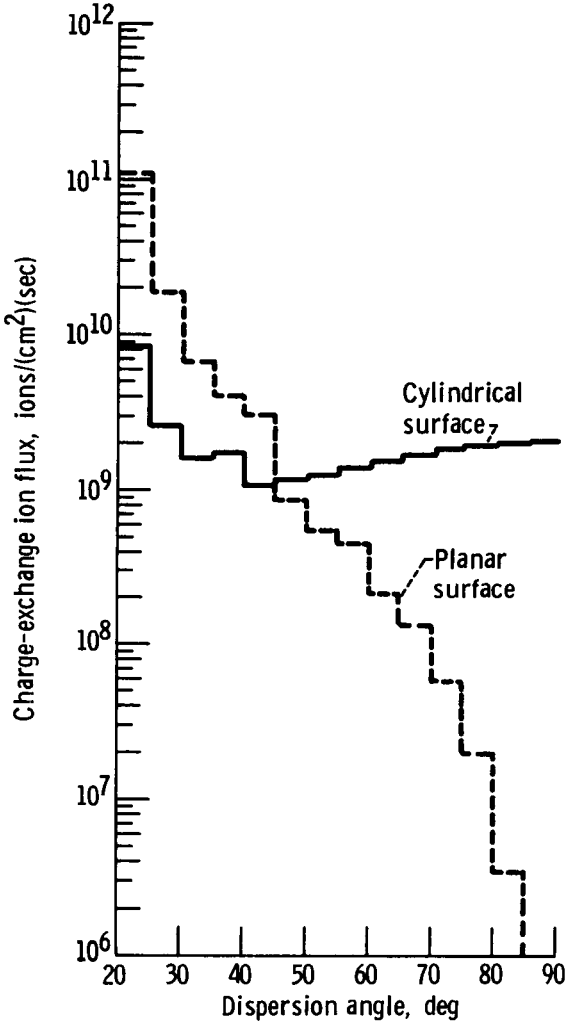

Figure 10. - Charge-exchange ion flux arriving at the two surfaces shown in figure 9.

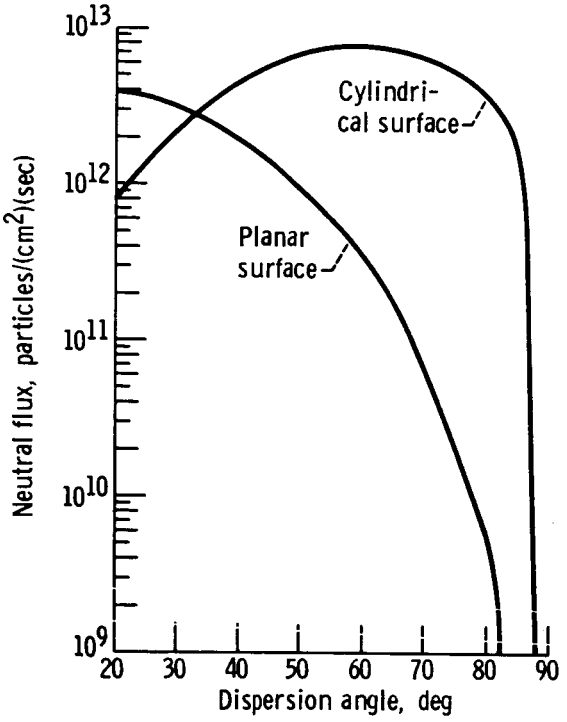

Figure 11. - Neutral flux arriving at the two surfaces shown in figure 9.